Detectability of the subdominant mode in a binary black hole ringdown

Swetha Bhagwat*
Department of Physics, Syracuse University, Syracuse, New York 13244, USA and Dipartimento di Fisica, Sapienza Universita di Roma, Sezione INFN Roma1, Piazzale Aldo Moro 5, 00185 Roma, Italy

Miriam Cabero
Department of Physics, Princeton University, Princeton, New Jersey 08544, USA

Collin D. Capano and Badri Krishnan
Max Planck Institute for Gravitational Physics (Albert Einstein Institute), Callinstrasse 38, D-30167 Hannover, Germany and Leibniz Universität Hannover, Welfengarten 1-A, D-30167 Hannover, Germany

Duncan A. Brown
Department of Physics, Syracuse University, Syracuse, New York 13244, USA

(Received 14 November 2019; revised 19 May 2020; accepted 3 June 2020; published 6 July 2020)

The ringdown is the late part of the postmerger signature emitted during the coalescence of two black holes and comprises a superposition of quasinormal modes. Within the general theory of relativity, the no-hair theorem for black holes states that the frequencies and the damping times of these modes are entirely determined by the mass and the angular momentum of the final Kerr black hole. Detection of multiple ringdown modes in the gravitational wave signal emitted during a binary black hole coalescence would allow us to validate the no-hair theorem with observations. The signal-to-noise ratio of the black hole ringdown and the amplitude of the subdominant modes to the dominant mode determine the detectability of the subdominant mode. We use Bayesian inference to investigate the interplay between these two factors towards their detectability. We systematically vary the two factors in a set of simulated analytical ringdown signals to infer the minimum signal-to-noise ratio needed in a ringdown signal for performing black hole spectroscopy. Our estimates on the minimum signal strength required to perform black hole spectroscopy as a function of amplitude ratio allows us to gain insight into the kind of signals that will be promising for black hole spectroscopy.

DOI: 10.1103/PhysRevD.102.024023

I. INTRODUCTION

The morphology of the gravitational wave signal from a binary black hole (BBH) merger is well known. Initially when the black holes are far apart, the signal is oscillatory with increasing amplitude and frequency; this part of the signal is well described by post-Newtonian theory. As the black holes get closer and merge to form a single remnant black hole, the post-Newtonian description breaks down. The amplitude reaches a maximum and then decreases as the remnant black hole approaches its equilibrium state, that of a Kerr black hole. At some point after the merger, the remnant black hole spacetime is sufficiently close to its final equilibrium state that it can be well modeled as a linear perturbation of a Kerr black hole. Power-law tails are expected at still later times, but these are likely too weak to be observable.

The equation governing the perturbation of a Kerr black hole can be cast in the form of a radiative boundary-value problem similar to a Schrödinger equation (though with a non-self-adjoint operator) with an effective potential depending on the mass M and specific angular momentum a of the black hole [1–5]. Imposing boundary conditions that are purely outgoing at infinity and purely infalling into the black hole horizon leads to exponentially damped sinusoidal solutions, the quasinormal modes (QNMs). For any given values of M and a, the frequencies $f_{n\ell m}(M,a)$ and damping times $\tau_{n\ell m}(M,a)$ of the QNMs are determined by three quantum numbers ℓ, m, n; ℓ and m are the angular quantum numbers while n denotes the overtones, i.e., number of zeroes of the radial part of the wave function.

If one were to observe a single QNM, then a knowledge of the mode indices ℓ, m, n would allow us to measure the mass and spin of the remnant black hole. It is reasonable to

*spbhagwa@syr.edu

assume that at sufficiently late times the least-damped mode will dominate, but this may not be true closer to the merger. It was found that the late time behavior of the first BBH merger detected by the LIGO detectors, GW150914, is consistent with the $\ell = m = 2, n = 0$ QNM [6] of the final black hole formed in this event.

This question is closely connected to the issue of quantifying the time after which the merging black hole spacetime can be treated perturbatively. By studying the $n = 0$ modes in numerical simulations of BBH mergers, it was suggested in Ref. [7] that starting from a time $\sim 10\ GM/c^3$ after the merger, the gravitational wave signal is consistent with the QNM frequencies calculated from black hole perturbation theory (this is also consistent with the observational result in Ref. [6]). This is further supported by an entirely different calculation, namely, the decay of the horizon multipole moments [8]; it is found that the decay rates of the horizon multipole moments become consistent with the QNM damping times roughly $10\ GM/c^3$ after the merger. See also Ref. [9] for a quantitative study of how the near horizon geometry approaches a Kerr solution and this study suggests a slightly later start time ($\sim 16\ GM/c^3$) for ringdown.

The general theory of relativity can be validated by checking the consistency of (M, a) between the ringdown and premerger portions of the signal [6,10,11]. However, the observation of frequencies and damping times of *multiple* ringdown modes would allow a more stringent test, and this is often referred to as black hole spectroscopy. As first proposed in Ref. [12], verifying the consistency of (M, a) measured from different modes independently allows us to test that the observations are consistent with the no-hair theorem. We note that one could also use information from the full inspiral-merger-ringdown models as presented in Ref. [13].

In a recent work, it is indicated that higher overtones might contribute closer to the merger [14] and can be used for black hole spectroscopy. This statement relies on the phenomenologically performing numerical fits of the post-merger signal with overtones and could be affected by parameter degeneracy. It could also be susceptible to overfitting, as shown in Ref. [15]. On the other hand, the decay rates of the multipole moments calculated in Ref. [8] are consistent with the higher overtones closer to the merger. The observation of higher overtones closer to the merger [16], if fully confirmed, makes the prospects for black hole spectroscopy very promising.

Traditionally, black hole spectroscopy has been studied using the angular modes in ringdown. Angular modes offer a particular advantage that they have a longer half-life (generally comparable to the dominant mode) compared to the overtones. From a data analysis perspective, the prospects of measuring a subdominant mode depend primarily on the overall signal-to-noise ratio (SNR) in the ringdown (ρ_{RD}) and the relative mode excitation amplitude ($A_R = A_{\mathrm{subdominant}}/A_{\mathrm{dominant}}$). For instance, a nearly equal mass BBH system like GW150914 does not excite the (asymmetrical) subdominant modes sufficiently and thus, is not ideal for inferring multiple modes in the ringdown. As a rule of thumb, the higher the asymmetry in the progenitor BBH system, the lower is the ρ_{RD} needed to detect the subdominant modes. This question, along with the related issue of resolving nearby frequencies and damping times, were previously studied using the Fisher matrix approximations (see, e.g., Refs. [17,18]). But more recently, in the era of gravitational wave detections, Bayesian parameter estimation techniques are used for parameter inferences from the detector data and several tool kits have been built specifically tailored towards gravitational wave astronomy (see, e.g., Refs. [19–21]). In this paper, we study the detectability of the subdominant ringdown mode in a Bayesian inference framework using the toolkit called PyCBC. Specifically, we study the effect of the amplitude ratio A_R and ρ_{RD} on detectability of the subdominant mode and provide an insight into what kind of BBH systems are likely to allow for multimode detectability in their ringdown signal. For this study, we assume that the underlying theory of gravity is the general theory of relativity and compute the frequencies and damping times as dictated by linear perturbation theory on the space-time of Kerr black hole formed during the BBH merger [22,23] for all the simulated signals used for this study.

Our goal is to provide an estimate of minimum SNR required in the ringdown as a function of amplitude ratio for a signal to be spectroscopically valuable. Further, we investigate the effect of A_R and ϕ_{33} in the detectability of the subdominant mode by systematically studying Bayesian parameter inference for a set of simulated ringdown signals. We specifically study the detectability of the subdominant mode in a full Bayesian parameter estimation setup on simulated signals to provide a lower limit on the SNR that is required to perform any 2-mode based ringdown tests.

This paper is organized in the following way: in Sec. II, we describe the ringdown waveform and the details of injections. Then, in Sec. III, we provide the setup for the Bayesian inference used for this study. This is followed by Sec. IV, where we present our results and, finally, we discuss its implications in Sec. V.

II. THE RINGDOWN WAVEFORM

For this study, we generate a simulated set of time-series data corresponding to BBH ringdown signals. In the limit when the wavelength of the signal is much larger than the size of the detector, it can be shown that the strain $h(t)$ observed by a detector is

$$h(t) = F_+(\alpha, \delta, \psi)h_+(t) + F_\times(\alpha, \delta, \psi)h_\times(t), \quad (1)$$

where $F_{+,\times}$ are the antenna patterns of the detector associated with the $+$ and the $\times$ polarizations of the

gravitational wave signal, $h_{+,\times}$, and depend on the location of the source with respect to the detector. The sky position of the source in the detector frame is described by the right ascension α and the declination δ, and the orientation of the preferred wave frame is represented by the polarization angle ψ.

The ringdown waveforms $h_{+,\times}$ can be expanded as a superposition of damped sinusoids

$$h_+ + ih_\times = \sum_{\ell,m,n} {}_2Y_{\ell m}(\iota,\varphi) A_{\ell mn} e^{i(\omega_{\ell mn} t + \phi_{\ell mn})}. \quad (2)$$

Here, ${}_2Y_{\ell m}$ are the spin-weighted spherical harmonics [24,25], $\omega_{\ell mn}$ is the complex QNM frequency calculated using the method of continued fractions developed in Ref. [22], $\phi_{\ell mn}$ the initial phase, and $A_{\ell mn}$ the (real) mode amplitude. For a perturbed Kerr black hole, although it is natural to use the spin-weighted spheroidal harmonics [5] instead of the spin-weighted spherical harmonics ${}_2Y_{\ell m}$, ${}_2Y_{\ell m}$ is, however, a good approximation up to moderately high BH spins (see, e.g., Ref. [26]).

In this paper, we shall restrict ourselves to the two loudest angular modes in a nonspinning BBH ringdown, and the one with the lower amplitude will be called the subdominant mode. We limit this study to the longest-lived overtone, i.e., $n = 0$, and therefore we drop the overtone index in the frequencies and damping times henceforward. For a BBH system comprising two nonspinning progenitor black holes, the loudest subdominant mode is known to be $\ell = m = 3$ for all mass ratios of BBHs [27,28]. Therefore, for simplicity, we consider only the $\ell = m = 2$ and $\ell = m = 3$ modes in this work. The QNM frequencies and damping times are determined uniquely by the mass M_f and specific angular momentum a_f of the final black hole formed. The $\ell = m = 2$ mode is the dominant mode with amplitude A_{22} and the subdominant (secondary) mode amplitude A_{33} will be parametrized via the amplitude ratio $A_R \coloneqq A_{33}/A_{22}$. Consequently, the waveform model we consider in this paper is fully described by six intrinsic parameters $\{M_f, a_f, A_{22}, A_R, \phi_{22}, \phi_{33}\}$.

III. THE PARAMETER ESTIMATION AND ITS IMPLEMENTATION

Bayesian inference provides a general framework for determining the parameters $\boldsymbol{\vartheta}$ of a BBH system through the posterior distributions $p(\boldsymbol{\vartheta}|\boldsymbol{\mathcal{D}},\mathcal{H})$ where $\boldsymbol{\mathcal{D}}$ is the time-series data and $\mathcal{H}$ is the model assumed. A signal from a BBH system is parametrized by a set of intrinsic parameters that affect the phase evolution of the signal (e.g., masses and spins), and by a set of extrinsic parameters (such as the sky position, luminosity distance, coalescence time, etc.) which affect the slowly varying amplitude. The signal model is then written as $h(t;\boldsymbol{\vartheta})$. Given a $\mathcal{H}$, one has expectations on the distribution of parameter values before performing an observation [29,30] encoded in a probability density function called the *prior*, $\mathcal{P}(\boldsymbol{\vartheta}|\mathcal{H})$. Once the observation is performed and the dataset is obtained, one updates the priors with information obtained from this observation. This input is encoded in the likelihood function $\mathcal{P}(\boldsymbol{\mathcal{D}}|\boldsymbol{\vartheta},\mathcal{H})$. The posterior probability density function $\mathcal{P}(\boldsymbol{\vartheta}|\boldsymbol{\mathcal{D}},\mathcal{H})$ for the parameters $\boldsymbol{\vartheta}$ is given by [29,30]

$$\mathcal{P}(\boldsymbol{\vartheta}|\boldsymbol{\mathcal{D}},\mathcal{H}) = \frac{\mathcal{P}(\boldsymbol{\vartheta}|\mathcal{H})\mathcal{P}(\boldsymbol{\mathcal{D}}|\boldsymbol{\vartheta},\mathcal{H})}{\mathcal{P}(\boldsymbol{\mathcal{D}}|\mathcal{H})}. \quad (3)$$

Here, $\mathcal{P}(\boldsymbol{\mathcal{D}}|\mathcal{H})$ is the *evidence* and serves as a normalization factor.

The likelihood function $\mathcal{P}(\boldsymbol{\mathcal{D}}|\boldsymbol{\vartheta},\mathcal{H})$ depends on both the signal and the nature of noise $\boldsymbol{\mathcal{N}}$ present in the data. If the noise model is Gaussian and stationary, the likelihood function $\mathcal{P}(\boldsymbol{\mathcal{D}}|\boldsymbol{\vartheta},\mathcal{H})$ can be written as

$$\mathcal{P}(\boldsymbol{\mathcal{D}}|\boldsymbol{\vartheta},\mathcal{H}) \propto e^{-\frac{1}{2}\langle \boldsymbol{\mathcal{N}}|\boldsymbol{\mathcal{N}}\rangle} = e^{-\frac{1}{2}\langle \boldsymbol{\mathcal{D}}-\mathcal{H}|\boldsymbol{\mathcal{D}}-\mathcal{H}\rangle}. \quad (4)$$

Here, $\langle .|.\rangle$ denotes an inner product in the space of signals written as

$$\langle x_i|y_i\rangle_i = 2\mathrm{Re}\int_0^\infty \frac{\tilde{x}_i^\star(f)\tilde{y}_i(f)}{S_n^{(i)}(f)} df. \quad (5)$$

The form of the prior distributions $\mathcal{P}(\boldsymbol{\vartheta}|\mathcal{H})$ is a choice that one has to make and there is no unique way to pick it. With the intention of extracting maximum information from the data itself, we use noninformative priors.

The noninformative priors used in this study are summarized below:

(i) M_f: Uniform between $[50, 100]\ M_\odot$.
(ii) a_f: Uniform between $[-0.99, 0.99]$.
(iii) A_{22}: Log-uniform between $[10^{-25}, 5\times10^{-20}]$.
(iv) A_R: Uniform between [0, 0.5].
(v) ϕ_{22} and ϕ_{33}: Uniform between $[0, 2\pi]$.

Note that a log-uniform prior on A_{22} is appropriate since the amplitude sets the scale of the ringdown signal. This choice also ensures a better sampling of the smaller amplitudes. On the other hand, since A_R is a ratio of amplitudes, a uniform prior is appropriate for it.

We perform a full Bayesian parameter estimation using the PyCBC package [21] to produce the posterior distribution for all the 6 ringdown parameters listed above. In practice, these posterior distributions[1] are computed by sampling [31] the allowed parameter space. We use the in-built implementation of the emcee_pt ensemble sampler to

[1]All the information about the distribution of the estimated parameters is contained in the landscape of $\mathcal{P}(\boldsymbol{\vartheta}|\boldsymbol{\mathcal{D}},\mathcal{H})$ and therefore, the goal of a scheme using Bayesian parameter estimation is to sample the parameters space of $\boldsymbol{\vartheta}$ and construct the distribution $\mathcal{P}(\boldsymbol{\vartheta}|\boldsymbol{\mathcal{D}},\mathcal{H})$ In most cases where one is just interested in estimating the parameter values for $\boldsymbol{\vartheta}$, $\mathcal{P}(\boldsymbol{\vartheta}|\boldsymbol{\mathcal{D}},\mathcal{H})$ is calculated up to a normalization factor. One need not compute the evidence to estimate the parameters of the model. Calculating the evidence is computationally challenging, especially when the parameter space spanned by $\boldsymbol{\vartheta}$ is large.

perform the parallel tempered Markov chain Monte Carlo (MCMC) operation [32–34]. The technical details of this algorithm are presented in Ref. [35]. We use 38 inverse-temperature chains to sample the parameter space. For each temperature chain, we use 200 walkers to explore the space. Also, we use an analytical model of the advanced LIGO sensitivity curve, named the zero-detuned-high power (ZDHP) noise curve,[2] for calculating the likelihood function at each sampled point.

We perform the parameter estimation for the 6 intrinsic ringdown parameters, $\{M_f, a_f, A_{22}, A_R, \phi_{22}, \phi_{33}\}$. All of the other extrinsic parameters are chosen arbitrarily and are held fixed throughout the study. The assumption is that these extrinsic parameters by themselves only depend on the propagation of gravitational radiation in our Universe, and not on intrinsic properties of the source, such as the validity of the no-hair theorem. In a more realistic case, these extrinsic parameters would be provided independently through the measurements done using the full GW signal from the event. We expect these extrinsic parameters to not have strong correlations to the recovery of the intrinsic parameters.

IV. RESULTS

A. Parameters of the injected signals

The injections used in this study contain two QNM modes of ringdown, with the frequencies and damping times fixed to be consistent with those of a Kerr QNM. In Refs. [28,36] fits for amplitudes of QNMs were performed using the postmerger in the numerical relativity simulations of BBH systems and these studies suggest that $\ell = m = 3$ is the loudest subdominant mode for all BBH mass ratio provided that the progenitor system comprises nonspinning black holes. Each injection used in this study comprises $\ell = m = 2, 3$. Note that the $\ell = 2$, $m = 1$ mode could be of comparable strength as the $\ell = m = 3$ for high mass ratio ($q \geq 6$) BBH and is particularly important when the progenitor BBH system has non-negligible black hole spins. Note, however, that the subdominant mode detectablility depends primarily on the overall $\rho_{\rm RD}$ and A_R and exact parameters of the BBH system effects only mildly—at the level of correlation of the parameters—the conclusions in this study. Although in this study we focus on the $\ell = m = 3$ subdominant mode detection, we expect the results to roughly hold for the $\ell = 2$, $m = 1$ mode too for the following reasons—(a) the damping times of the $\ell = 2$, $m = 1$, $n = 0$, and $\ell = m = 3$ are comparable and this ensures that for a given value of A_R the power contained in both the subdominant mode is comparable, (b) the frequency difference between the both these angular mode with the dominant mode is comparable (∼100 Hz) for a GW150914-like system), suggesting a similar kind of parameter correlations. Furthermore, neither of them have significant issues with resolvablity from the fundamental mode as studied in Ref. [28].

Moreover, unlike in the case of a full inspiral-merger-ringdown signal, where the merger dynamics are governed by the nonlinear space-time evolution predicted by general relativity, our injections are a sum of QNMs as predicted by the linear perturbation theory. Our study does not rely on the choice of start time as our signal model is fully consistent with linear perturbation theory. A followup study needs to be performed on the numerical relativity postmerger to access the influence of the choice of start time of ringdown. Throughout this study we assume that the SNR content in the part of the postmerger signal considered as ringdown, i.e., the portion of the signal after the chosen start time, is denoted by $\rho_{\rm RD}$.

Our simulated ringdowns correspond to a black hole with $\{M_f = 70\ M_\odot, a_f = 0.65\}$, similar to the remnant formed in the GW150914 event. During the first and second observing runs of LIG0/Virgo detectors, final BH mass in the range $M_f \in [17, 80]\ \odot$ were observed [37]. From the perspective of the detectablility of a subdominant mode in the ringdown, the choice of M_f determines the temporal scaling of the signal, and thereby the SNR contained in the ringdown. Therefore, we quantified our results in terms of $\rho_{\rm RD}$ and A_R and we do not expect the choices of parameters of the BH to significantly effect any of our conclusions.

Along the same line of argument, we fix the values of the extrinsic parameters for all of our injections.

(i) Inclination angle: $\iota = 0.7$ rad.
(ii) Right ascension and declination: $\alpha = 2.2$ rad, $\delta = -1.24$ rad.
(iii) Polarization angle: $\psi = 0.3$ rad.
(iv) Initial phases: $\phi_{22} = 0$, $\phi_{33} = 1$ rad.

These choices are arbitrary and they either affect the value of $\rho_{\rm RD}$ [as in the case of (α, δ)] or A_R (as in the case of ι). Figure 3 of Ref. [17] presents the effect of the choice of ι on the observed amplitudes of QNM; we note that our choice of $\iota = 0.7$ rad is fairly favorable for viewing the subdominant mode. However, since our results are parametrized in terms of A_R and $\rho_{\rm RD}$, we highlight that these choices do not affect our results.

Further, we perform these injections in zero noise. Zero noise is a realization of Gaussian noise and therefore any assumption during the PE that relies on the nature of noise being Gaussian still remains valid. However, a more detailed followup work of a similar nature needs to be performed in the presence of detector noise to understand the influences of noise in a realistic scenario. This is beyond the scope of our current study. Here, we aim to provide a lower bound for the SNR in the ringdown that is required for detection of the subdominant mode and provide optimistic quantitative results.

We consider 16 combinations of the optimal ringdown SNR $\rho_{\rm RD}$ and the mode amplitude ratio $A_R = A_{33}/A_{22}$ in

[2] https://dcc.ligo.org/LIGO-T1800044/public

this study. In particular, we focus on ringdown signals corresponding to the following values of $\rho_{\rm RD}$ and A_R.

(i) $\rho_{\rm RD} = \{15, 20, 25, 30\}$.
(ii) $A_R = \{0, 0.1, 0.2, 0.3\}$.

Note that for a fixed choice of ι, the value of A_R is determined by the mass ratio and the spins of the progenitor BBH system. Therefore, this results' dependence on A_R for detectablity can be used to gain an insight into the kind of BBH system that will allow for black hole spectroscopy using angular modes in ringdown. For moderate values of the mass ratio, studies show that it is not unreasonable to have $A_R = \mathcal{O}(10^{-1})$, which motivates our choice of the values for A_R listed above [38–40].

B. Detectability of the subdominant mode

To study the detectability of the subdominant mode, we infer the intrinsic parameters, i.e., $\{M_f, a_f, A_{22}, A_R, \phi_{22}, \phi_{33}\}$, for each of the simulated ringdowns described in Sec. II using a Bayesian parameter estimation framework. For each case, we find that the 90% credible interval of the posterior distribution contains the injected values of all the parameters. As an example of parameter recovery, we provide the posterior distribution for the inference of final mass and spin corresponding to our least favorable ringdown simulation, i.e., $A_R = 0.1$ and $\rho_{\rm RD} = 15$, in Fig. 1.

We define a subdominant mode as "detectable" in the ringdown if the 90% credible interval of the recovered posterior distribution for A_R excludes $A_R = 0$. Since we aim to focus on the detectability of the subdominant mode in ringdown, henceforward we focus only on the recovered posterior distributions of the mode amplitude ratios and the phases.

In Appendix, we present the recovered posterior distribution of A_R and ϕ_{33} along with 50% and 90% credible intervals for all the simulations used in this study. Figure 6 show posteriors for A_R, ϕ_{33} with varying $\rho_{\rm RD}$ and A_R. We find that the injected value of A_R, ϕ_{33} (indicated by blue line in the figures) lies within the 50% (and thus, 90%) credible interval for all the simulations. Further, in Fig. 2, we present "the null tests," where the injection contains only one mode, i.e., $A_R = 0$. Further from the plots presented in the Appendix, we confirm that this holds true for single mode injection of varying strengths, i.e., we find that the posterior distribution indeed rails against $A_R = 0$ and no information on ϕ_{33} is obtained.

Among the injections we studied, the most unlikely candidate to allow for detection of the subdominant mode is $A_R = 0.1$ and $\rho_{\rm RD} = 15$ (top right panel of Fig. 2). For this case, $A_R = 0$ is not excluded from the 90% credible interval from the posterior distribution and, therefore, the presence of the subdominant mode cannot be inferred. For the ease of comparison, we present the joint posterior distribution for $A_R - \phi_{33}$ for the case of $A_R = 0.1$, $\rho_{\rm RD} = 15$ and the null test side by side in Fig. 2. We note that the posterior distribution for A_R has more support for higher values of A_R compared to the null test. Further, it is striking that the marginalized posterior distribution of ϕ_{33} peaks around the injected value of ϕ_{33}, even for the most unfavorable cases considered in our study. This feature should be explored further in a future work and could serve as a hint for the possible presence of the subdominant mode with a low amplitude.

Moreover, we confirm that as $\rho_{\rm RD}$ increases, the posterior distribution for A_R shifts towards the injected values of $A_R = 0.1$ and the phase of the $l = m = 3$ modes is better inferred. Since the population studies of BBH favor nearly equal mass BBH systems [41] where the asymmetrical

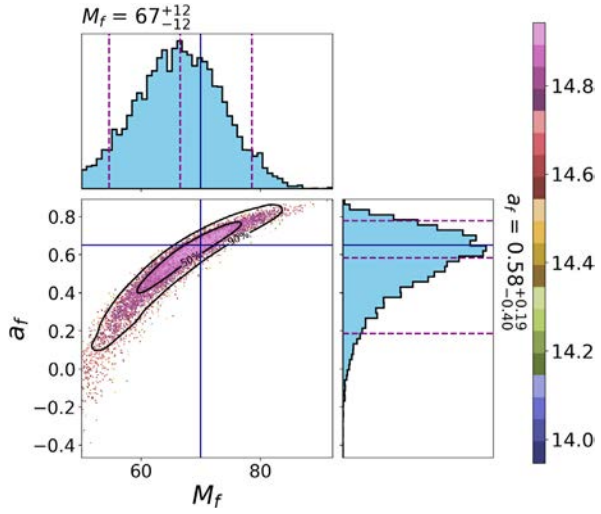

FIG. 1. Final mass and spin recovery. This plot presents the recovery of final mass M_f and final spin a_f for the case of $\rho_{\rm RD} = 15$ and $A_R = 0.1$. Although we provide the posterior probability distribution $M_f - a_f$ for just one case, we would emphasize that recovery of the mass and spin have similar behavior for all the cases (including the single mode null tests).

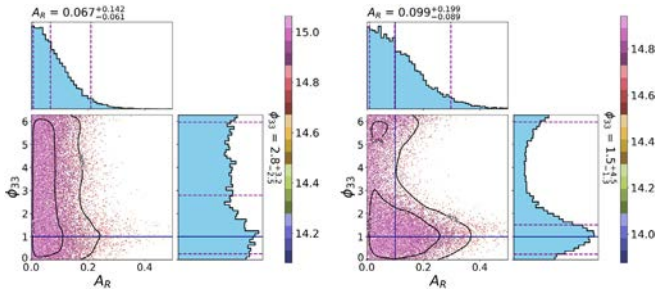

FIG. 2. The joint posterior distributions of A_R-ϕ_{33} obtained for injections with $A_R = 0$(left), 0.1(right) corresponding to $\rho_{\rm RD} = 15$. The left panel is the null test and the right panel has an injection where the subdominant mode does not satisfy our criterion for detecability. In this figure we would like to highlight that even when the subdominant mode is not detectable, the shape of the posterior hints towards the presence of the subdominant mode.

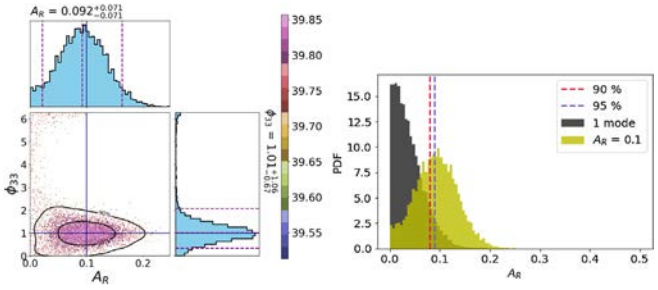

FIG. 3. Parameter estimation results for the $A_R = 0.1$ case with the SNR increased to $\rho_{\mathrm{RD}} = 40$. (Left) Posterior distribution for the amplitude ratio and phase of the subdominant mode. (Right) Comparison of the marginalized posterior distribution of the amplitude ratio for $A_R = 0$ (black) and $A_R = 0.1$ (green).

subdominant mode is not excited sufficiently, studying the RDs for smaller A_R is crucial. We therefore perform an injection followed by parameter estimation with $\rho_{\mathrm{RD}} = 40$ for the $A_R = 0.1$ event. We present the posterior distribution inferred for this case in Fig. 3. In this case, we find that we indeed infer the presence of the subdominant mode.

Also, in plots presented in Appendix, higher A_R and ρ_{RD} allows for detectability of the subdominant mode confidently. For instance, for the simulation corresponding to $A_R = 0.3$, the 90% credible interval of the posterior distribution of A_R excludes zero clearly even for $\rho_{\mathrm{RD}} = 15$. The joint posterior distribution illustrating this is shown in Fig. 4. For quantitative comparison, we tabulate the 90% highest posterior density (HPD) credible interval on the marginalized PDF of A_R for all our simulations in Table I. In the table, we use bold type for the simulations that pass our criterion for detectability of the subdominant ringdown mode. We see that for $A_R = 0.1$ the detection of a subdominant mode cannot be claimed confidently (for $\rho_{\mathrm{RD}} \leq 30$). However, for $A_R = 0.2$, we can infer the presence of the subdominant mode with $\rho_{\mathrm{RD}} \geq 20$. And, finally, for $A_R = 0.3$, we can infer the presence of the second mode for all the injections used in this study, including $\rho_{\mathrm{RD}} = 15$.

Next, we access the interplay between the false alarm and the false dismissal probabilities for the inferred presence of the subdominant mode in these cases. This will provide an intuition towards the goodness of the

TABLE I. 90% highest posterior density (HPD) credible interval on the marginalized PDF of A_R. In bold type are the cases where we are able to infer the presence of the subdominant mode. Posterior distributions are shown in Fig. 6.

ρ_{RD}	$A_R = 0.1$	$A_R = 0.2$	$A_R = 0.3$
15	$6.6 \times 10^{-8} - 0.24$	$1.4 \times 10^{-5} - 0.35$	**0.122–0.49**
20	$1.4 \times 10^{-5} - 0.19$	**0.04–0.34**	**0.16–0.46**
25	$5 \times 10^{-5} - 0.17$	**0.08–0.32**	**1.18–0.43**
30	$\mathbf{1.2 \times 10^{-4} - 0.16}$	**0.1–0.3**	**0.2–0.4**

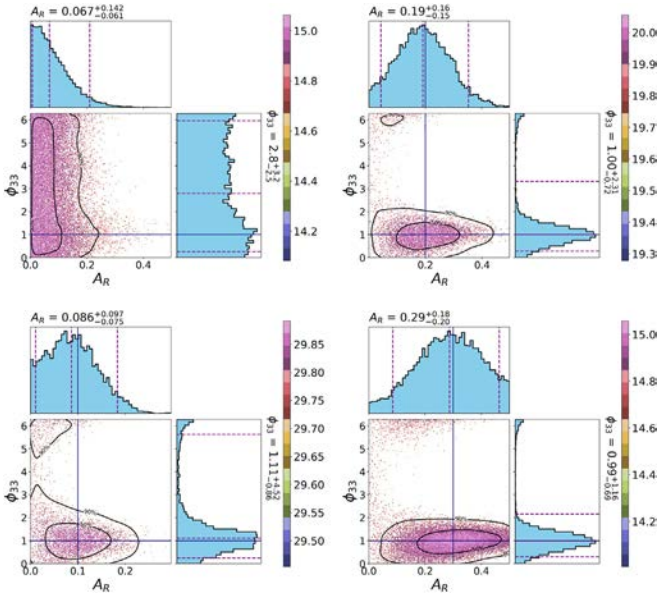

FIG. 4. The joint posterior distributions of A_R-ϕ_{33} obtained for injections with $A_R = 0$(top, left), 0.1(bottom, left), 0.2(top, right), 0.3(bottom, right) corresponding to each of their minimum SNR required to detect the subdominant mode. This corresponds to a SNR $\rho_{\mathrm{RD}} = 15$, 30, 20, 15 for $A_R = 0$, 0.1, 0.2, 0.3, respectively.

criterion used to infer the presence and absence of the mode. We compare the marginalized posterior distributions for A_R at different SNR with the null case to access the false alarm and false dismissal probabilities. In Fig. 5 we show the marginalized posterior distributions for A_R. The panels are arranged from top to bottom for $\rho_{\mathrm{RD}} = 15$, 20, 25, 30, respectively, and different colors correspond to values of A_R in the injections.

To define the false dismissal probability β, we need to choose a threshold on A_R based on the null case. The thresholds $A_R^{90\%}$ and $A_R^{95\%}$ correspond, respectively, to 90% and 95% false alarm rates and these are shown as vertical lines in Fig. 5. For any of these thresholds, say $A_R^{90\%}$, the false dismissal probability is

$$\beta^{90\%} = \int_0^{A_R^{90\%}} p(A_R|\hat{A}_R) dA_R, \tag{6}$$

where $\hat{A}_R$ is the true injected value of A_R. If the posterior distribution for A_R of the injected simulations separates out (does not have large support for A_R smaller than the false alarm threshold value) from the posterior distribution of the null test, i.e., $A_R = 0$, the presence of the subdominant mode can be inferred confidently. We note that the posterior distributions corresponding to $A_R = 0.3$ (pink) always separates from $A_R = 0$ (black), even for $\rho_{\mathrm{RD}} = 15$, whereas that which corresponds to $A_R = 0.2$ (the blue histogram) separates out after $\rho_{\mathrm{RD}} = 20$. Table II lists the values of β for all the cases considered for this study and these results

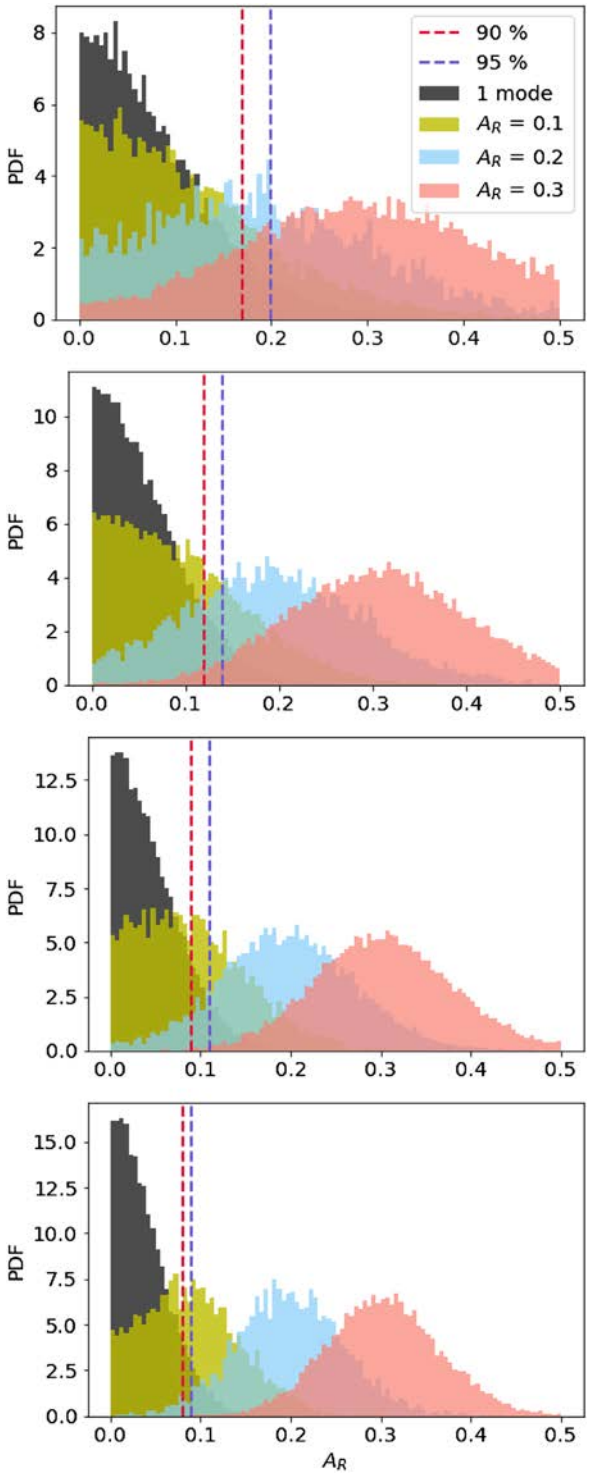

FIG. 5. Marginalized posterior distributions of the amplitude ratio for all the injections in this study. From top to bottom, the ringdown injections have optimal SNR $\rho_{\mathrm{RD}} = \{15, 20, 25, 30\}$, respectively. The black histograms correspond to the null case, where the injected signal has only one mode. The green, blue, and red histograms correspond to the injection with amplitude ratio of $A_R = \{0.1, 0.2, 0.3\}$, respectively. We claim the detection of a second mode when the colored histograms (corresponding to a nonzero amplitude ratio) separate clearly from the black histogram.

TABLE II. False dismissal probability $\beta^{90\%}$ for detection of a nonzero value of A_R for different values of the SNR and injected amplitude A_R.

ρ_{RD}	$A_R = 0.1$	$A_R = 0.2$	$A_R = 0.3$
15	0.75	0.46	0.17
20	0.67	0.23	0.02
25	0.53	0.07	1.6×10^{-3}
30	0.45	0.02	10^{-4}

are consistent with the credible intervals listed in Table I. Note also that for the case of $A_R = 0.1$, the posterior distribution (green) of A_R does not separate from the null test cases, thus not allowing for confident detection of the subdominant mode at a $\rho_{\mathrm{RD}} \sim 30$. However, when we increase ρ_{RD} to 40, we find that the presence of subdominant mode can be inferred confidently for simulation with $A_R = 0.1$. This result is presented in the left panel of Fig. 3.

From our study, we conclude that the minimum signal strength required for a confident detection on the subdominant mode depends largely on the amplitude ratio between the modes. We find the minimum of $\rho = \{40, 20, 15\}$ is required for the detection of the subdominant modes for the signal with mode amplitude ratio $A_R = \{0.1, 0.2, 0.3\}$, respectively. A_R is determined by the property of the BBH system and hence, these results can be used to gain insight into the kind of signals that will be promising for performing BH spectroscopy. The excitation amplitude of the different modes depends on the perturbation conditions set up by the inspiral-merger phase. This, in turn, is dictated by the asymmetry of the BBH system, i.e., the mass ratio q and the spin of the progenitor BHs χ. More asymmetric BBH systems have higher subdominant modes excitation amplitudes. If the BBH system comprises nonspinning BHs, then the value of A_R is determined by the mass ratio q of the component BH. $A_R = 0.1$ maps to a BBH system with $q \sim 1.5$, $A_R = 0.2$ to $q \sim 2.5$, and $A_R = 0.3$ to $q \sim 5$. Therefore, our result indicates for a BBH with $q \sim 1.5$, a loud ringdown with $\rho_{\mathrm{RD}} \sim 40$ will be required to detect a subdominant angular mode confidently.

V. DISCUSSIONS AND IMPLICATIONS

BH spectroscopy can validate the no-hair theorem with observational GW data and requires confident detection of multiple ringdown modes. In this paper, we have applied Bayesian inference techniques to the problem of *detecting* a sub-dominant ringdown mode for different values of the ringdown SNR ρ_{RD} and mode amplitude ratio A_R. The minimum SNR required to claim detection of subdominant mode is dependent on the amplitude ratio between the modes which, in turn, depends on to the initial BBH parameters like mass ratio and initial BH spins. A BBH system with a low mass ratio like the GW150914 ($q \sim 1.22$) would require a high value of ringdown SNR

($\rho_{\rm RD} \geq 40$) to detect the subdominant mode. In particular, we find that if a nonspinning BBH with mass ratio $q \sim 1.5$ were to produce a remnant similar to that formed GW150914 event, a SNR of $\rho_{\rm RD} \sim 40$ is required to detect the subdominant mode.

Further, for this study, we have taken the $\ell = m = 2, n = 0$ and $\ell = m = 3, n = 0$ modes to be the dominant and subdominant modes, respectively. For a nonspinning BBH system, $\ell = m = 3, n = 0$ is the loudest subdominant mode [27,28]. However, if the progenitor BHs had non-negligible spins, then for certain mass ratios $\ell = 2$, $m = 1$, $n = 0$ can be louder than or comparable to the excitation of $\ell = m = 3, n = 0$ mode. It would be straightforward to extend it to include other choices for the subdominant modes, including higher overtones in a similar framework. However, given that the subdominant mode frequencies are well separated (∼80–100 Hz) from the dominant mode frequency for both $\ell = 2, m = 1, n = 0$ and $\ell = m = 3, n = 0$ and the damping times are of the same order of magnitude, we do not expect the qualitative behavior of the posterior distribution of A_R to change significantly. The results presented in this paper are based on the posterior distributions inferred for A_R and ϕ_{33} and, therefore, we expect our result to not change significantly.

For a BBH ringdown signal, the excitation amplitude of the different modes depends on the perturbation conditions set up by the inspiral-merger phase. This, in turn, is dictated by the asymmetry of the initial BBH system, i.e., mass ratio and the spin of the progenitor. Generally speaking, more asymmetric systems will have higher modes excited but are also less likely to be detected.

Asymmetrical BBH systems produce ringdown with a larger value of A_R but are also less likely to be detected [37,42,43]. The general question of how likely we are to detect a sufficiently asymmetric system with networks of future gravitational wave detectors, and the issue of determining the frequencies and damping times rather than just detecting them, will be addressed in a companion paper [44].

Lastly, we would like to highlight that the quantitative values for the SNR provided for detectability of the subdominant modes in this study are optimistic lower bounds. This study is performed in noiseless data and with the assumption that the underlying theory of gravity is GR, i.e., we derive the QNM frequencies expected in GR. We sample for the final mass and spin of the BH instead of the QNM frequencies and damping time and this reduces the parameter space for Bayesian inference, thereby allowing the detection of the second mode at a smaller SNR. However, we would like to highlight that in the situations when the SNR in the ringdown is not sufficiently high to extract the values of frequencies and damping times of the subdominant modes reliably, obtaining the posterior distribution for $\{M_f, a_f, A_{22}, A_R, \phi_{22}, \phi_{33}\}$ under the assumption they are QNM as dictated by GR provides a valuable information in itself and acts as a null hypothesis test. If there is a deviation of the signal from what is predicted by GR, it is expected to be reflected as features of posterior distribution; for example, one might observe features like multimodal posterior for final mass and spin if the frequency for the second mode is significantly different from the GR predictions. Another interesting analysis in the case of low SNR would be comparing the variance of the inferred posteriors from the GW data with that of a simulated signal injected in similar signal-to-noise levels.

Although the setup we have used already sheds light on our assumption that the underlying theory is GR, a more robust test of GR would require measurement of the QNM frequencies and damping times directly from the data. Using a Fisher matrix framework combined with the Rayleigh criterion as presented in Ref. [17] a rough lower bound of SNR required for resolving the ringdown modes are $\rho_{\rm RD} \sim 25$, 13, 9 for $A_R = \{0.1, 0.2, 0.3\}$, respectively. In future work, we plan to investigate the measurement of subdominant mode frequencies and damping time in a fully Bayesian framework.

ACKNOWLEDGMENTS

We would like to thank Alexander H. Nitz and Steven Reyes for useful discussions. S. B. and D. A. B. thank National Science Foundation Grant No. PHY-1707954 for support. S. B. acknowledges financial support provided under the European Union's H2020 ERC, Starting Grant Agreement No. DarkGRA757480 and networking support by the COST Action CA16104 and from the Amaldi Research Center funded by the MIUR program Dipartimento di Eccellenza (CUP: B81I18001170001). M. C. acknowledges support from National Science Foundation Grant No. PHY-1607449, the Simons Foundation, and the Canadian Institute For Advanced Research (CIFAR). Computations were supported in part through computational resources provided by Syracuse University, supported by National Science Foundation Grant No. ACI-1541396, and by the Atlas computer cluster at the Albert Einstein Institute (Hannover).

APPENDIX: POSTERIOR DISTRIBUTION OF A_R AND ϕ_{33}

In Fig. 6, we provide the joint posterior distribution for A_R-ϕ_{33} for all the injections used for this study. Note the interplay of A_R and $\rho_{\rm RD}$ on the shape of the posterior probability distribution as well as on the spread of the 90% and 50% credible interval. The color bars in each of these panels correspond to the recovered SNR and the blue lines indicate the injection parameters. The top row in the figure corresponds to "the null test," where the

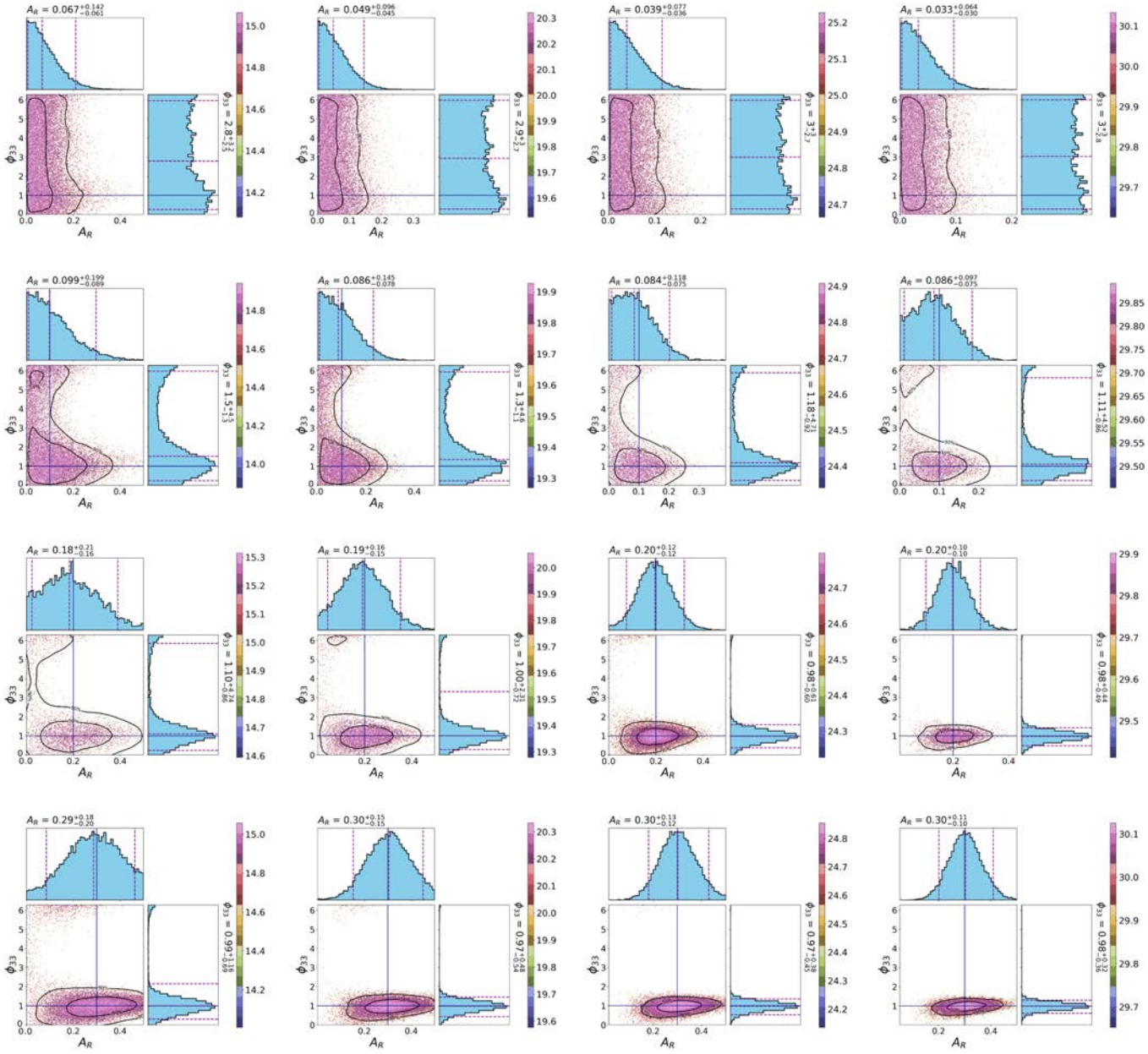

FIG. 6. Posterior distributions for the amplitude ratio A_R and phase of the subdominant mode ϕ_{33} for all the cases investigated in this study. The purple lines indicate the injected values in each of these cases. From top to bottom, the rows correspond to $A_R = 0$, 0.1, 0.2, 0.3 and from left to right the columns correspond to $\rho_{\rm RD} = 15$, 20, 25, 30.

injections contains only one mode, i.e., $A_R = 0$. The second, third, and fourth row correspond to $A_R = 0.1$, 0.2, and 0.3, respectively. The columns in the panel correspond to injections with $\rho_{\rm RD} = \{15, 20, 25, 20\}$ from left to right. In each of these cases, we find that the injected values of the parameters (indicated by the red line in the figures) lie within the 50% (and thus, 90%) credible interval. Further, the null tests in Fig. 6 are consistent with what is expected; the marginalized posterior for A_R rails against $A_R = 0$, thereby, indicating the absence of the second mode. Also, no information on the phase of $l = m = 3$ mode can be inferred for this case.

[1] S. A. Teukolsky, Astrophys. J. **185**, 635 (1973).
[2] W. H. Press and S. A. Teukolsky, Astrophys. J. **185**, 649 (1973).
[3] S. A. Teukolsky and W. H. Press, Astrophys. J. **193**, 443 (1974).
[4] C. V. Vishveshwara, Nature (London) **227**, 936 (1970).
[5] S. Chandrasekhar, *The Mathematical Theory of Black Holes*, Oxford Classic Texts in the Physical Sciences (1985).
[6] B. P. Abbott *et al.* (Virgo and LIGO Scientific Collaborations), Phys. Rev. Lett. **116**, 221101 (2016).
[7] I. Kamaretsos, M. Hannam, S. Husa, and B. S. Sathyaprakash, Phys. Rev. D **85**, 024018 (2012).
[8] A. Gupta, B. Krishnan, A. Nielsen, and E. Schnetter, Phys. Rev. D **97**, 084028 (2018).
[9] S. Bhagwat, M. Okounkova, S. W. Ballmer, D. A. Brown, M. Giesler, M. A. Scheel, and S. A. Teukolsky, Phys. Rev. D **97**, 104065 (2018).
[10] A. Ghosh *et al.*, Phys. Rev. D **94**, 021101 (2016).
[11] M. Cabero, C. D. Capano, O. Fischer-Birnholtz, B. Krishnan, A. B. Nielsen, A. H. Nitz, and C. M. Biwer, Phys. Rev. D **97**, 124069 (2018).
[12] O. Dreyer, B. Kelly, B. Krishnan, L. S. Finn, D. Garrison, and R. Lopez-Aleman, Classical Quantum Gravity **21**, 787 (2004).
[13] R. Brito, A. Buonanno, and V. Raymond, Phys. Rev. D **98**, 084038 (2018).
[14] M. Giesler, M. Isi, M. Scheel, and S. Teukolsky, Phys. Rev. X **9**, 041060 (2019).
[15] S. Bhagwat, X. J. Forteza, P. Pani, and V. Ferrari, Phys. Rev. D **101**, 044033 (2020).
[16] M. Isi, M. Giesler, W. M. Farr, M. A. Scheel, and S. A. Teukolsky, Phys. Rev. Lett. **123**, 111102 (2019).
[17] E. Berti, J. Cardoso, V. Cardoso, and M. Cavaglia, Phys. Rev. D **76**, 104044 (2007).
[18] M. Shahram and P. Milanfar, IEEE Trans. Signal Process. **53**, 2579 (2005).
[19] J. Veitch *et al.*, Phys. Rev. D **91**, 042003 (2015).
[20] G. Ashton *et al.*, Astrophys. J. Suppl. Ser. **241**, 27 (2019).
[21] C. M. Biwer, C. D. Capano, S. De, M. Cabero, D. A. Brown, A. H. Nitz, and V. Raymond, Publ. Astron. Soc. Pac. **131**, 024503 (2019).
[22] E. W. Leaver, Proc. R. Soc. A **402**, 285 (1985).
[23] E. Berti and V. Cardoso, Phys. Rev. D **74**, 104020 (2006).
[24] J. N. Goldberg, A. J. MacFarlane, E. T. Newman, F. Rohrlich, and E. C. G. Sudarshan, J. Math. Phys. (N.Y.) **8**, 2155 (1967).
[25] I. M. Gelfand, R. A. Minlos, and Z. Y. Shapiro, *Representations of the Rotation and Lorentz Groups and their Applications* (Pergamon Press, New York, 1963).
[26] E. Berti and A. Klein, Phys. Rev. D **90**, 064012 (2014).
[27] L. London, D. Shoemaker, and J. Healy, Phys. Rev. D **90**, 124032 (2014).
[28] X. Jiménez Forteza, S. Bhagwat, P. Pani, and V. Ferrari, arXiv:2005.03260.
[29] L. Xiang, IIE Transactions **39**, 829 (2007).
[30] A. Gelman, J. Carlin, H. Stern, D. Dunson, A. Vehtari, and D. Rubin, *Bayesian Data Analysis*, 3rd ed. (Chapman & Hall/CRC Texts in Statistical Science) (Chapman and Hall/CRC, London, 2014).
[31] W. G. Cochran, *Sampling Techniques*, 3rd ed. (John Wiley, New York, 1977).
[32] D. van Ravenzwaaij, P. Cassey, and S. D. Brown, Psychon. Bull. Rev. **25**, 143 (2018).
[33] D. W. Hogg and D. Foreman-Mackey, Astrophys. J. Suppl. Ser. **236**, 11 (2018).
[34] J. M. Flegal, M. Haran, and G. L. Jones, Stat. Sci. **23**, 250 (2008).
[35] D. Foreman-Mackey, D. W. Hogg, D. Lang, and J. Goodman, Publ. Astron. Soc. Pac. **125**, 306 (2013).
[36] L. T. London, arXiv:1801.08208.
[37] A. H. Nitz, C. Capano, A. B. Nielsen, S. Reyes, R. White, D. A. Brown, and B. Krishnan, Astrophys. J. **872**, 195 (2019).
[38] S. Bhagwat, D. A. Brown, and S. W. Ballmer, Phys. Rev. D **94**, 084024 (2016).
[39] L. London, D. Shoemaker, and J. Healy, Phys. Rev. D **90**, 124032 (2014).
[40] S. Borhanian, K. G. Arun, H. P. Pfeiffer, and B. S. Sathyaprakash, arXiv:1901.08516.
[41] B. P. Abbott *et al.* (LIGO Scientific and Virgo Collaborations), Astrophys. J. **833**, L1 (2016).
[42] A. H. Nitz, T. Dent, G. S. Davies, S. Kumar, C. D. Capano, I. Harry, S. Mazzon, L. Nuttall, A. Lundgren, and M. Tápai, Astrophys. J. **891**, 123 (2020).
[43] B. P. Abbott *et al.* (LIGO Scientific and Virgo Collaborations), Phys. Rev. X **9**, 031040 (2019).
[44] B. P. Abbott *et al.* (LIGO Scientific and Virgo Collaborations), Astrophys. J. **882**, L24 (2019).